Biosensors and Bioelectronics 47 (2013) 80–85

Contents lists available at SciVerse ScienceDirect

Biosensors and Bioelectronics

journal homepage: www.elsevier.com/locate/bios

Cascaded nano-porous silicon for high sensitive biosensing and functional group distinguishing by Mid-IR spectra

Minh-Hang Nguyen [a], Hau-Jie Tsai [b], Jen-Kuei Wu [a], Yi-Shiuan Wu [a], Ming-Chang Lee [c], Fan-Gang Tseng [a,d,*]

[a] Department of Engineering and System Science, National Tsing Hua University, Hsinchu, Taiwan, R.O.C.
[b] Department of Life Science, National Tsing Hua University, Hsinchu, Taiwan, R.O.C.
[c] Department of Electrical Engineering, National Tsing Hua University, Hsinchu, Taiwan, R.O.C.
[d] Division of Mechanics, Research Center for Applied Sciences, Academia Sinica, Taipei, Taiwan, R.O.C.

ARTICLE INFO

Article history:
Received 7 January 2013
Accepted 4 February 2013
Available online 15 March 2013

Keywords:
Porous silicon
RI sensor
FTIR
Chemical sensor
Biosensor

ABSTRACT

We present a chemical-biosensor in the Mid-IR range and based on cascaded porous silicon made on p- and n-type (100) silicon substrates of resistivities between 0.001 Ω cm and 0.005 Ω cm. The stacked porous layers of various porosities (20–80%) and thicknesses (5–9 μm) are formed by successive electrochemical etchings with different current densities. Working with FTIR technique that possesses fast response, high sensitivity, and capability of detecting and identifying functional groups, the cascaded porous structures provided enhanced refractive index sensitivities and reduced detection limits in chemical and biodetection. The largest wavenumber shifts were 50 cm^{-1}/mM obtained for D-(+)-glucose and 96 cm^{-1}/μg/mL for Cy5-conjungated Rabbit Anti-Mouse IgG. The lowest detectable concentration of glucose was 80 μM (1.4 mg/mL) with PS porosity of 40% and thickness of about 9 μm while it was 40 ng/mL for Cy5-conjugated Rabbit Anti-Mouse IgG which is 2.5×10^5 folds better than those in literature.

© 2013 Elsevier B.V. All rights reserved.

1. Introduction

Porous silicon (PS) has been widely used in chemical and biosensing due to its high sensitivity like for detection of binding of IgG to a protein A-modified surface (Dancil et al., 1999), ethanol vapors (Salem et al., 2007), water and liquid ethanol (Torres-Costa et al., 2005) and 3-aminopropyltriethoxysilane (Wei et al., 2008). The main enhancing factor of PS devices results from high porosity providing increased volume for liquid analytes and area for membrane analytes. So far many PS-based chemical and biosensors have been reported working in the visible (300–800 nm) and near infrared (NIR) (1000–2000 nm) ranges with typical sensitivities in a range of 60–300 nm/RIU (Salem et al., 2007; Torres-Costa et al., 2005), and a highest sensitivity of 1090 nm/RIU (Wei and Weiss, 2011) was also reported. But few works reported PS-based chemical and biosensors working in the middle infrared (Mid-IR) range of 2500–25,000 nm. PS-based sensors working in the Mid-IR range should offer some important advantages such as a large amount of biomolecules can be accommodated by the large pore volume and these Mid-IR devices are also compatible with traditional Fourier Transform Infrared (FTIR) spectroscopy. FTIR provides powerful detection capability in chemical and biosensing because of its rapid sampling, high signal-to-noise ratio, ability to quickly identify (detecting and assigning) characteristic peak wavenumbers to functional groups in chemical and bio substances (Duygu et al., 2009; Gorga, 1989; Kong and Yu, 2007; Movasaghi et al., 2008; Ozturk et al., 2007; Stuart, 2012).

To incorporate advantages of PS structure and FTIR spectrometry, we proposed to use PS devices working in a reflectance configuration where an analyte in the PS layers could be exposed to the FTIR light source, and the reflected light from the devices could be caught by FTIR detector and provide information about the analyte. The reflection spectra are very informative carrying characteristic wavenumber peaks corresponding to different molecular bonds (functional groups) in analytes, and the signal can be further enhanced by PS modulation for high sensitive detection. With the PS-based device, an analyte can cover the device surface as well as penetrate into the thick porous layer leading to large change of effective RI of the device. Thus a large shift is observed in the spectra. Sensitivity is therefore much enhanced. Spectrometer FTIR-4000 (JASCO, USA) using MCT-M detector cooled with liquid nitrogen was employed throughout the experiments.

We used the electrochemical etching (ECE) method (Chen et al., 2011; Fauchet, 2007; Föll et al., 2002; Lehmann et al., 2000; Ouyang and Fauchet, 2005; Smith and Collins, 1992) to prepare PSs on p- and n-type (100) silicon substrates whose resistivities were in a range from 0.001 Ω cm to 0.005 Ω cm for porosity

* Corresponding author at: Department of Engineering and System Science, National Tsing Hua University, Hsinchu, Taiwan.
E-mail addresses: fangang@ess.nthu.edu.tw, minhhang@ess.nthu.edu.tw (F.-G. Tseng).

0956-5663/$ - see front matter © 2013 Elsevier B.V. All rights reserved.
http://dx.doi.org/10.1016/j.bios.2013.02.006

ranging from 20% to 80%. The devices then were tested for D-(+)-glucose with concentrations ranging from 20 mM/mL down to 0.2 mM/mL and for Cy5-conjugated Rabbit Anti-Mouse IgG with concentrations ranging from 10 μg/mL down to 1 ng/mL.

2. Materials and methods

2.1. Materials

- p-type (boron) and n-type (phosphor) (100) silicon wafers with resistivity in a range between 0.001 and 0.005 Ω cm were used. The wafers were cleaned with acetone, IPA and piranha (H_2SO_4: H_2O_2), then rinsed with deionized (DI) water. Buffered oxide etch (BOE) etching was carried out for 1 min to remove thin silicon dioxide (SiO_2) layer on the top, and DI water rinse was done before heating the wafers at 120 °C on hotplate for 10 min. A photolithography step was done to define etching area (1 cm^2) on the polished side of silicon wafers and another was done to define a top gold ring-shaped electrode surrounding the etching area. The silicon wafers were then cut into small pieces for further etching.
- Analyte Group 1: D-(+)-glucose, abbreviated as GC, was purchased from Sigma-Aldrich. The analyte was diluted with DI water to have different concentrations of 20 mM, 5 mM, 1 mM and 0.2 mM.
- Analyte Group 2: 3-Aminopropyltriethoxysilane, abbreviated as 3-APTES and Cy5-conjugated Rabbit Anti-Mouse IgG, abbreviated as Cy5-IgG, were purchased from Sigma-Aldrich.
- All other chemicals were purchased from Sigma-Aldrich if no information is given.

2.2. The electrochemical etching method

ECE gives flexible pore sizes and porosity ranges dependent on numerous parameters such as silicon type, doping level, and current density. Moreover, this method allows the formation of multilayer porous structures with different porosities controlled by alternating current densities and different thicknesses controlled by etching time sequentially (Harraza et al., 2008; Ouyang et al., 2005). Porosities ranging from 20% to 80% with pore sizes ranging from 10 nm to over 1 μm can be fabricated by the ECE method (Harraza et al., 2008). High porosity allows a large amount of analyte to be absorbed and exist in the porous layers that enhance signals. Different pore sizes can be used for different bioagents with molecule sizes ranging from several nanometers to a few micrometers.

Potentiostat CHI-760B Electrochemical Workstation (CH Instruments, Inc., USA) with 3 electrode configuration was used to fabricate PS structures. As a working electrode, the silicon samples had a gold ring-shaped electrode on the top side. The top-side electrode was set surrounding a round window to be etched. Since in our experiments resistivity of the silicon samples was low (0.001–0.005 Ω cm), an alternative placement was also used where the copper working electrode was attached directly to the bottom of the silicon samples with no necessity of the top gold ring. It helps reducing one photolithograph step on the one side and keeping etching areas uniform on the other side. A thin platinum (Pt) reference electrode with a diameter of 0.5 mm was placed at a distance of about 1 cm above the silicon sample, and another spiral Pt electrode was used as a counter electrode to provide uniform current density. The HF-based etching solution combines of 15% HF (49%) in pure ethanol (99.5%) and 1000 ppm surfactant NCW-1001 (Wako Pure Chemical Industries, Ltd., Japan) contained in a teflon chamber. All etchings were carried out at room temperature. After etching, the samples were sent to a furnace for oxidation at 500 °C for 5 min or 900 °C for 3 min. It was to make the sample surfaces hydrophilic to facilitate absorption of analytes in Group 1 and to enhance bonding of 3-APTES in Group 2.

2.3. Pore size and porosity evaluation

Gravimetry (Fekih et al., 2006) is a common method to estimate porosity of PSs, but it must be carried out carefully to ensure accurate results (for example identical sample dryness, environment humidity, and temperature effect). Also, this method cannot give the information of pore size and morphology. As a result, direct measurement on the images of the structures is an appropriate method for evaluating both porosity and pore size of PSs with vertical hole structures. In the pore size evaluation, PS samples are cut and cleaned before being dried and coated with a thin gold layer for SEM picturing. Average pore size and porosity are evaluated by direct measurement of the width of vertical tracks (holes) and silicon walls in the SEM crosssection view images. For more accurate results, the average pore size and porosity are calculated by image processing. Scanning probe image processor SPIP, version 4.0.0.0 (Image Metrology, Denmark) with function “Gain/Pore Analysis” was used to estimate porosity and pore size of PS samples from their SEM top view images.

2.4. Spectrometry for RI detection

In spectrometry, analytes are directly dispensed onto sensors to obtain specific spectra. The spectra are reconstructed by spectrometers and analyzed by spectroanalyzers. RI value, signal strength, and spectrum shift are the three major parameters for characterizing the analyses. (Beheiry et al., 2010; Harraza et al., 2008; Nazirizadeh et al., 2010; Ouyang et al., 2005).

In most traditional works, analytes were detected with sensors working in the visible and NIR ranges. In our work, the devices were tested in the Mid-IR range with FTIR-4000. In bioanalyzing, FTIR technique is used widely for identifying (assigning) functional groups/fingerprint wavenumbers of the analytes. As mentioned above, we specially used FTIR-4000, simultaneously taking the advantages of both RI change and functional groups recognition via molecule vibration in the Mid-IR range. Moreover, the RI sensitivity measured in a longer wavelength range (for example the Mid-IR range) is usually higher than that measured in a shorter wavelength range (for example the visible range). Therefore we can not only detect RI change with high sensitivity but also identify the functional group(s) that exist in biomatters. In this paper, we acquired Mid-IR spectra from PSs for detecting different concentrations of GC and Cy5-IgG.

2.5. Cascaded PS structures for chemical and biosensing

Fig. 1(a) shows the schematic of a cascaded PS structure consisting of several alternate layers, the porosities of which are obtained by applying different current densities and the thicknesses are controlled by etching time. The number of PS layers, their porosities and thicknesses are designed to ensure the device working well in the Mid-IR range. The designing is not discussed in this paper, but it can be found in literatures (Wang and Magnusson, 1995; Wei and Weiss, 2011). The device spectra for two analytes are schematically shown in Fig. 1(b). The device spectrum for an analyte with an RI (for example, RI1) will shift to a longer wavelength (lower wavenumber) for another analyte with a higher RI (RI2 > RI1). The device structures and their spectra in GC and Cy5-IgG will be shown and discussed in more detail in Section 3.2.

3. Results and discussion

3.1. Porous silicon etching

The etching took place from the edge towards the center and etched fringes could be observed for the first tens of seconds. With longer etching time (after about 40 s) the etched area became more uniform. The reason results from the higher initial etching rate at the edge area than that at the inner area. This phenomenon can be seen in Fig. 1 in the Supplementary material. Fig. 2 shows SEM cross-section images of p-type PS samples etched with current densities in a range between 20 mA/cm^2 and 80 mA/cm^2 for intermediate pore sizes ranging from 50 nm to 100 nm. The etching conditions and properties of these samples are summarized in Table 1.

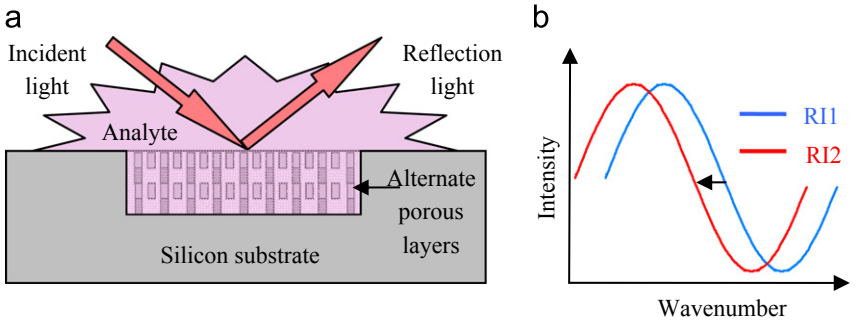

Fig. 1. Schematics of a PS device under testing (a) and its spectra in two analytes (RI1 < RI2) (b).

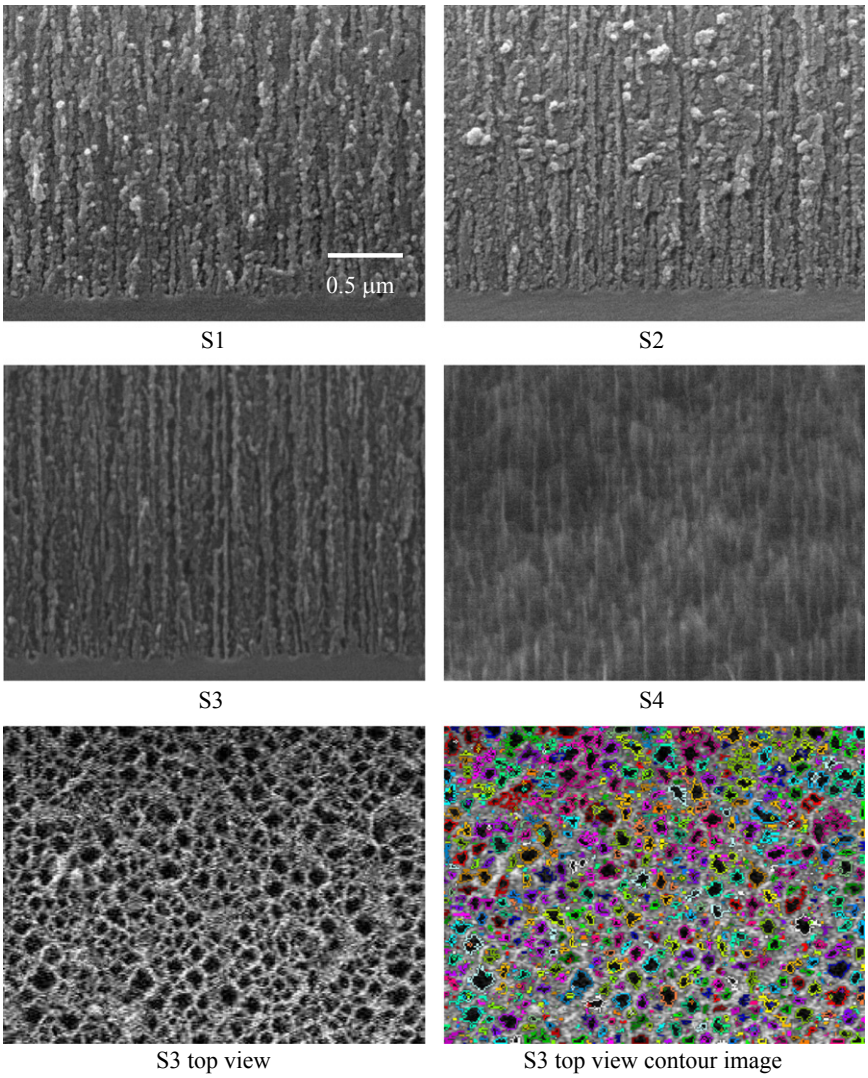

Fig. 2. SEM cross-section view images of PS samples formed by etching p-type (100) Si, resistivity of 0.001 Ω cm, by the ECE method with electrolyte mixed of HF(49%): ethanol(99.5%)=25:58.3v/v, current densities of 20 mA/cm^2, 40 mA/cm^2, 60 mA/cm^2, and 80 mA/cm^2 for samples S1, S2, S3, and S4, respectively. All etchings were carried out at room temperature for 300 s. Scale bar is 0.5 μm for all images. S3 SEM top view image and S3 contour image obtained with SPIP software are examples for evaluating pore size and porosity.

Since resistivity of silicon samples used in our work was low (0.001–0.005 Ω cm), the size of formed pores was small, ranging from a few nanometers to several tens of nanometers with current density varying from 10 to 80 mA/cm^2, respectively. In ECE etching, there is a typical phenomenon where PS is covered by a very dense layer, which may be about 1 μm thick with pore size of 5–10 nm (Harraza et al., 2008; Ouyang et al., 2005). The lower layers have a more steady porosity depending on the etching current density. Fig. 3 shows two porous layers of a p-type PS sample obtained by etching alternatively with a current density of 10 mA/cm^2. The top layer (Fig. 3(a)) had a dense upper part (near surface) with pore diameter of about 5–10 nm, and a more porous lower part follows. The lower layer (Fig. 3(b)) had a more uniform morphology with a pore diameter of about 40 nm. To have the desired uniform cylindrical pores, silicon samples need to be pre-patterned (thin porous layer is slightly patterned and removed) before porous etching. The formed pores would be larger and more uniform.

The same etching parameters were applied for etching n-type silicon samples with resistivity in a range between 0.001 and 0.005 Ω cm giving the average pore size in a range from 70 nm to 230 nm. The formed PS samples on n-type had pore size larger than that of p-type silicon samples, for example, the average pore sizes in p- and n-type PS samples were about 70 nm and 225 nm, respectively, by using the same current density of 40 mA/cm^2.

Table 1
p-type PS samples etched in ECE with different current densities.

Sample	Current density (mA/cm^2)	Etching time (s)	Porous layer thickness (μm)	Porosity (%)	Refractive index[a]
S1	20	300	5.0	10	2.887
S2	40	300	5.36	25	2.013
S3	60	300	5.88	40	1.719
S4	80	300	7.28	65	1.517

[a] Referenced based on Wei et al. (2008).

3.2. Spectrometry results

GC analyte with different concentrations was used to test the PS chips with FTIR-4000 that can scan wavenumber ranging between 4000 and 400 cm^{-1} (the wavelength range from 2.5 to 25.0 μm). Cy5-IgG was also used for testing the PS samples. The analytes were applied on the surface of the PS devices and their FTIR spectra were obtained to estimate their characteristics. PS sample P1, and P2 (p-type) had total porous structure thickness of about 8.6 μm including 20 alternate layers of 25% and 40% porosities (formed by current densities of 40 mA/cm^2 and 60 mA/cm^2, respectively) and one layer with porosity of 65% (current density of 80 mA/cm^2) in the center as a "defect" layer. Samples N1 and N2 (n-type) had total porous structure thickness of about 7 μm including 12 alternate layers of 69% and 58% porosities (formed by current densities of 40 mA/cm^2 and 34 mA/cm^2, respectively) and one porous layer with porosity of 69% (formed by current density of 40 mA/cm^2) in the center as a defect layer. Fig. 4(a) shows etching potential-time plot for multilayer porous samples P1 and P2. Fig. 4(b) shows SEM image of P1 that consisted of 20 alternate layers with porosities of about 25% and 40% and one defect layer with porosity of about 65% in the center.

After etching, the p-type and n-type PS samples were oxidized at 500 °C for 5 min and 900 °C for 3 min, respectively, to keep the surface stable for testing and enhance the absorption of GC solutions

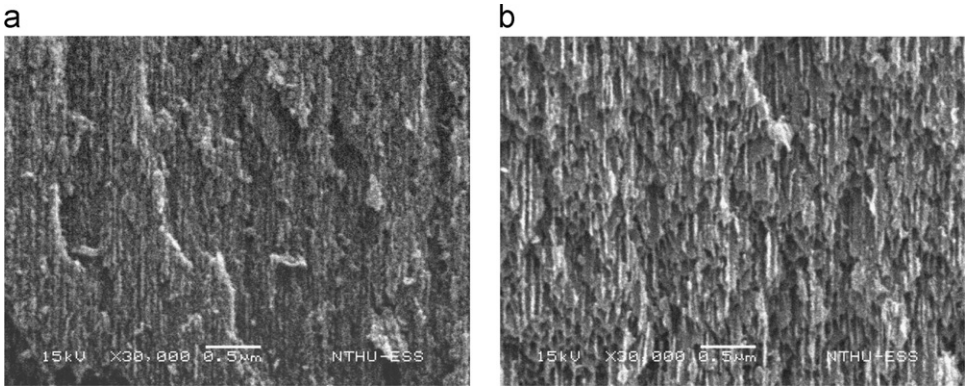

Fig. 3. SEM images of two porous layers made alternatively in a p-type sample etched with current density of 10 mA/cm^2. The top layer had pore size of 5 nm on the upper part and 10 nm at the lower part (a), while the lower layer had average pore size of 40 nm (b). Scale bar is 0.5 μm in both images.

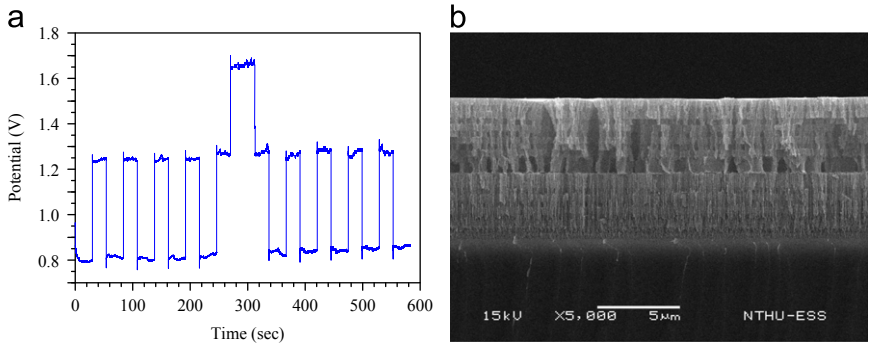

Fig. 4. Etching potential-time plot of PS–P1 (a) and its SEM image of crosssection view (b). The PS structure consisted of 20 alternate layers of two different porosities (25% and 40%) and one defect layer (65%) in the center. The total thickness of porous structure was about 8.6 μm.

as well as the bonding of bioanalytes (3-APTES, Cy5-IgG). Due to oxidation, Mid-IR spectra of p-type PS samples showed the blue-shifts of 200 nm. With DI water (RI 1.3334) filled in PS sample, red shifts of 193 nm was recorded corresponding to a sensitivity of 579 nm/RIU. Fig. 5(a) and (b) shows FTIR reflection spectra of P1 and P2 with GC of different concentrations at 0.2 mM, 1 mM, 5 mM, and 20 mM diluted with DI water, respectively. The average sensitivity of P1 was about 23 cm^{-1}/mM while it was about 50 cm^{-1}/mM for P2. Remarkably, though P1 and P2 were etched at the same current density and duration, the etching solution for P2 was more diluted than that for P1, therefore pore size of P2 was larger than that of P1 (Harraza et al., 2008), with thicker porous layers, resulting in larger shift of P2 spectra.

The shifts were not linear with higher sensitivity for lower GC concentrations. For an average sensitivity of 50 cm^{-1}/mM for GC, the typical resolution set as 4 cm^{-1} gave a LOD of 80 μM (1.4 mg/mL). High resolution of 0.5 cm^{-1} (the highest resolution of FTIR-4000) could give a LOD of 10 μM (0.18 mg/mL). Only 1 μL or less of analyte was required for a PS device with porous area of 1 cm^2 and porous thickness of 10 μm. The characteristics of the devices are better than some reported sensors using different principles of measurement (Hovhannisyan, 2008; Toghill and Compton, 2010; Wei and Weiss, 2011) and reported in previous IR based sensors with 9.4 mg/mL (Kwak et al., 2012) and 4 mg/mL (Brandstetter et al., 2010).

With larger pores (average size was 225 nm), two similar n-type PS samples N1 and N2 (porosity 64%) were employed for 3-APTES/Cy5-IgG testing. These PS samples fabricated with the same set of parameters had very close porosity and porous structures. Like p-type samples, these oxidized samples had blue-shifts due to the PS surface RI changes in oxidation, with visible and Mid-IR blue-shifts of 62 nm and 300 nm, respectively. With DI water filled in the PS samples, red-shifts of 162.53 nm for visible and 268 nm for Mid-IR spectra were recorded corresponding to a sensitivity of 488 nm/RIU and 805 nm/RIU, respectively, much higher than previous works. There was also observed a high and broad peak at a low wavenumber range (the central wavenumber was about 1260 cm^{-1}) associated with some characteristic group directly related to SiO_2 layers formed in oxidation. With the oxidation temperature higher

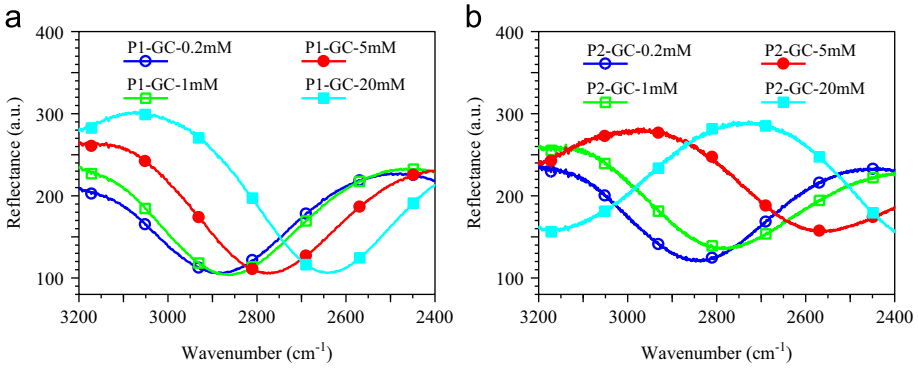

Fig. 5. FTIR reflection spectra of PS samples P1 (a) and P2 (b) with different concentrations of GC as 0.2 mM, 1 mM, 5 mM and 20 mM in DI water.

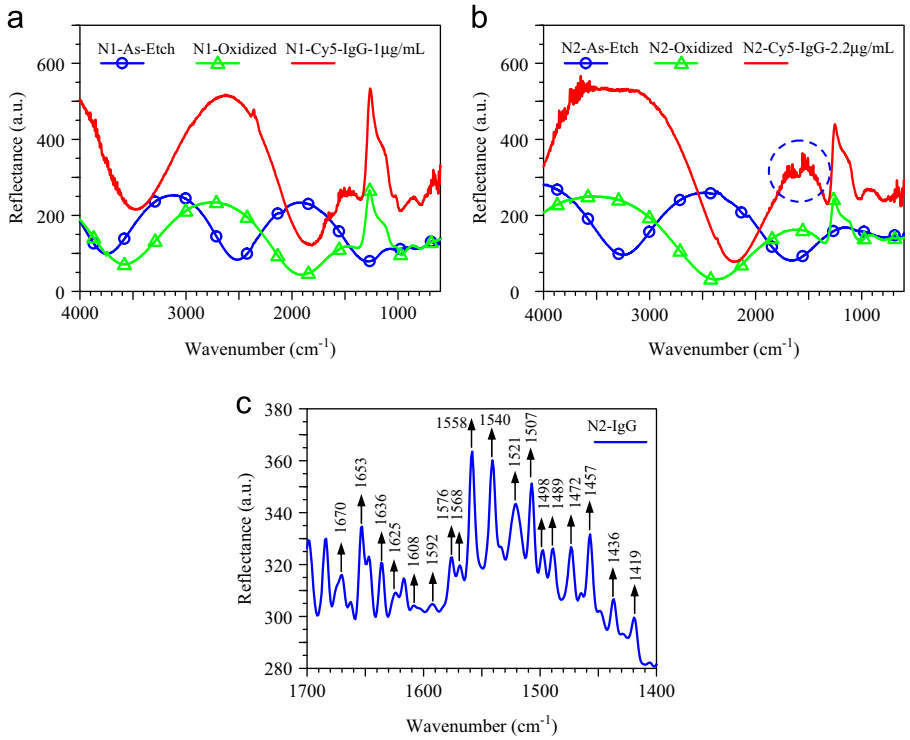

Fig. 6. (a) FTIR reflectance spectra of n-type PS samples N1 (a) and N2 (b) after sequential steps: as-etched, oxidation, and Cy5-IgG coating (c) enlarged view of a N2's portion (in dashed blue circle) for assignment of functional groups existing in the sample. (For interpretation of the references to color in this figure legend, the reader is referred to the web version of this article.)

"oxide peaks" showed higher intensity. Fig. 6(a) and (b) shows FTIR reflection spectra of the samples N1 and N2 after three steps: etching, oxidation and coating 3-APTES/Cy5-IgG. The presence of 3-APTES/Cy5-IgG in porous samples N1 and N2 introduced many tiny peaks superimposed on the reflection spectra at the high, medium and low wavenumber ranges of 3600–4000 cm^{-1}, 1870–1330 cm^{-1}, and lower than 750 cm^{-1}, respectively, that were related to the functional groups in bound molecules, particularly 3-APTES, Cy5-IgG. Some of the peak wavenumbers ranged between 1400 cm^{-1} and 1700 cm^{-1} shown in Fig. 6(c) were assigned as listed in Table 1 in the Supplementary material of the paper.

N2 had a red-shift of 180 cm^{-1} for Cy5-IgG at a concentration of 2.2 μg/mL while N1 had a red-shift of 96 cm^{-1} for Cy5-IgG at a concentration of 1 μg/mL. Thus when the concentration nearly doubles, the amount of shift almost doubles as well, indicating approximately the same sensitivity in these two PS samples. Moreover, FTIR reveals more intensive characteristic peaks of N2 over N1 as seen in Fig. 2(c) in the Supplementary material. Therefore when concentration increases, FTIR reveals more intensive characteristic peaks while the PS structures provide larger spectrum shift. The combined uses of PS structures and FTIR spectrometry support each other in chemical and biodetection.

Besides testing similar devices N1 and N2 with the two different Cy5-IgG concentrations of 1 μg/mL and 2.2 μg/mL, respectively, another testing was done with the same Cy5-IgG concentration of 2.2 μg/mL for n-type device N3 with porosity of 40%. The device N3 showed sensitivity of 52 cm^{-1}/1 μg/mL lower than that of N2 with porosity of 64%.

With FTIR resolution set typically at 4 cm^{-1}, LOD of PS devices like N2 was about 40 ng/mL of Cy5-IgG while it was about 77 ng/mL for devices like N3. Thus their sensitivities and LODs were much better than those reported in previous works (Kong and Yu, 2007) where no PS structure but FTIR spectroscopy was used and concentration needed to be higher than 10 mg/mL to obtain a high quality protein spectrum.

Our "cascaded" porous structure was in fact a 1D photonic crystal (PhC) with a certain bandwidth. With a central defect layer a sharp resonance peak/dip would appear in the bandgap. This resonance dip would allow high resolution and clear distinction hence reducing LOD. Our current PS structures had bandgap and resonance dip in the visible region, therefore in these experiments the advantage of the resonance dips was still unrevealed. In our future works the band gap and its resonance dip will designed in Mid-IR, and sensors' LOD will be promised being improved further.

4. Conclusion

This work has introduced a cascaded nano-porous silicon based chips as sensing elements working with FTIR reflection spectrometry for chemical and bio substances detection. The sensor sensitivity is greatly enhanced, and the fingerprints of related functional groups can be well-characterized by these devices for biomolecule detection. The PSs were made on p-type and n-type (100) silicon substrates with low resistivity (0.001–0.005 Ω cm) by electrochemical etching to obtain pore size ranging from 50 nm to 200 nm and thickness of 5–9 μm. PS samples were tested with D-(+)-glucose and gave a very high sensitivity as 50 cm^{-1}/mM and low LOD as 80 μM (1.4 mg/mL), that is about 2.8 folds higher than described in previous works. For Cy5-conjugated Rabbit Anti-Mouse IgG, the PS samples gave the sensitivity of 96 cm^{-1}/1 μg/mL and LOD of 40 ng/mL which is 2.5×10^5 folds better than those in the previous works.

Acknowledgment

This work was supported under projects NSC99-2120-M-007-009, NSC 99-2113-M-007-017, NSC-100-2120-M-007-006, and NSC-100-2627-M-007-013. We appreciate the help and discussions from Prof. Chih-Hao Lee and Prof. Yu-Chuan Su, in NTHU ESS department and the instrument training from Dr. Hsin-Yi Hsieh, Judy M. Obliosca, Yi-Chuan Chen, and Kai-Ning Ku.

Appendix A. Supporting information

Supplementary data associated with this article can be found in the online version at http://dx.doi.org/10.1016/j.bios.2013.02.006.

References

Beheiry, M.E., Liu, V., Fan, S., Levi, O., 2010. Optics Express 18 (22), 22701–22714.
Brandstetter, M., Genner, A., Anic, K., Lend, B., 2010. Analyst 135 (12), 3260–3265.
Chen, C.Y., Duong, H.P., Wong, C.C., Yen, T.Y., 2011. Journal of the Electrochemical Society 158 (5), D302–D306.
Dancil, K.P.S., Greiner, D.P., Sailor, M.J., 1999. Journal of the American Chemical Society 121, 7925–7930.
Duygu, D.Y., Baykal, T., Acikgoz, I., Yidiz, K., 2009. Gazi University Journal of Science 22 (3), 117–121.
Fauchet, P.M., 2007. Biophotonics Winter School.
Föll, H., Christophersen, M., Carstensen, J., Hasse, G., 2002. Materials Science and Engineering R 39, 93–141.
Fekih, Z., Otmani, F.Z., Ghellai, N., Chabanne-Sari, N.E., 2006. Moroccan Journal of Condensed Mater 7 (1), 35–37.
Gorga, J.C., 1989. Proceedings of the National Academy of Science USA 86, 2321–2325.
Harraza, F.A., El-Sheikh, S.M., Sakka, T., Ogat, Y.H., 2008. Electrochimica Acta. 53, 6444–6451.
Hovhannisyan, A.S., 2008., pp. 38–42, ⟨http://ajp.asj-oa.am/32/1/Bio-sens-AJP.pdf⟩.
Kong, J., Yu, S.N., 2007. Acta Biochimica et Biophysica Sinica 39 (8), 549–559.
Kwak, Y.H., Choi, D.S., Kim, Y.N., Kim, H., Yoon, D.H., Ahn, S.S., Yang, J.W., Yang, W.S., Seo, S., 2012. Biosensors and Bioelectronics 37, 82–87.
Lehmann, V., Stengl, R., Luigart, A., 2000. Materials Science and Engineering B 69–70, 11–22.
Movasaghi, Z., Rehman, S., Rehman, I.U., 2008. Applied Spectroscopy Reviews 43, 134–179.
Nazirizadeh, Y., Bog, U., Sekula, S., Mappes, T., Lemmer, U., Gerken, M., 2010. Optics Express 18 (18), 19120–19128.
Ouyang, H., Fauchet, P.M., 2005. SPIE Optics East.
Ouyang, H., Christophersen, M., Viard, R., Miller, B.L., Fauchet, P.M., 2005. Advanced Functional Materials 15, 1851–1859.
Ozturk, N., Tabak, A., Akgo, S., Denizli, A., 2007. Colloids and Surfaces A: Physicochemical and Engineering Aspects 301, 490–497.
Salem, M.S., Sailor, M.J., Harraz, F.A., Sakka, T., Ogata, Y.H., 2007. Physica Status Solidi (c) 4 (6), 2073–2077.
Smith, R.L., Collins, S.D., 1992. Journal of Applied Physics 71 (8), R1–R22.
Stuart, B.H., 2012. Published online: 15.06.12, doi:10.1002/9780470027318.a0208.pub2.
Toghill, K.E., Compton, R.G., 2010. International Journal of Electrochemical Science 5, 1246–1301.
Torres-Costa, V., Agulló-Rueda, F., Martín-Palma, R.J., Martínez-Duart, J.M., 2005. Optical Materials 27, 1084–1087.
Wang, S.S., Magnusson, R., 1995. Applied Optics 34 (14), 2414–2420.
Wei, X., Kang, C., Liscidini, M., Rong, G., Retterer, S.T., 2008. Journal of Applied Physics 104, 123111–123113.
Wei, X., Weiss, M., 2011. Optics Express 19 (12), 11330–11339.